

Correlation of lithospheric velocity and electrical conductivity for Southern Africa

Alan G. Jones¹, Stewart Fishwick², Rob L. Evans³, and The SAMTEX Team⁴

1: Dublin Institute for Advanced Studies, 5 Merrion Square, Dublin, Ireland, alan@cp.dias.ie;

2: Department of Geology, University of Leicester, University Road, Leicester, LE1 7RH, U.K.;

3: Department of Geology and Geophysics, Woods Hole Oceanographic Institution, Clark 263, 266 Woods Hole Rd, MA 02543, U.S.A.;

4: Other members of the SAMTEX team include: Louise Collins, Xavier Garcia, Colin Hogg, Clare Horan, David Khoza, Marion Miensopust, Mark Muller, Pieter-Ewald Share, Jessica Spratt, Gerry Wallace (DIAS); Alan D. Chave (WHOI); Sue Webb (Wits); Janine Cole, Patrick Cole, Raimund Stettler (CGS); Tiyyapo Ngwisany, G. Tshoso (GSB); David Hutchins (GSN); Shane Evans, Hielke Jelsma (De Beers); Theo Aravanis, Andy Mountford, Ed Cunion (RTME); Wayne Pettit, David Khoza (BHP-B); Stoffel Fourie, Pieter-Ewald Share (CSIR); Jan Wasborg (ABB)

ABSTRACT

Southern Africa is the world's premier location for studying the Sub-Continental Lithospheric Mantle (SCLM) given the abundance of geophysical and geochemical data that now exist for it. In particular, the Southern African Seismic Experiment (SASE) and the Southern African Magnetotelluric Experiment (SAMTEX) have added a wealth of seismological and electrical data that can be explored for physical property information and compared and contrasted both qualitatively and quantitatively. Qualitatively there is significant spatial correlation between low velocity and low resistivity regions and between high velocity and high resistivity regions. Adopting a quadratic relationship between shear-wave velocity and resistivity, based on mineral physics arguments, and predicting the velocity from the observed resistivity shows that the two are compatible except for two distinct regions. This relationship requires that resistivity be controlled by bulk property effects, particularly temperature variation, and not by minor conductive phases.

Key words: SAMTEX, SASE, electrical resistivity, seismic velocity.

INTRODUCTION

Imaging the structures and geometries within the Sub-Continental Lithospheric Mantle (SCLM) that are a consequence of formation and deformation processes offers clues to its tectonic history. Southern Africa is the world's premier natural laboratory for studying and testing theories about Archean and Proterozoic SCLM processes given the abundance of geophysical and geochemical data that exist for it. The former as a consequence of many prior studies and more recently the 1996-1998 Southern African Seismic Experiment (SASE, black dots on Fig. 1) and the 2004-2008 Southern African Magnetotelluric Experiment (SAMTEX, coloured dots on Fig. 1), that together have added a wealth of seismological and electrical data, and the latter from studies of the extensive xenolith samples brought to the surface by kimberlitic magmas. Focussing on the geophysical information, but utilizing the geochemical and petrological data, the SASE and SAMTEX data can be explored for physical property information and compared and contrasted both qualitatively and quantitatively.

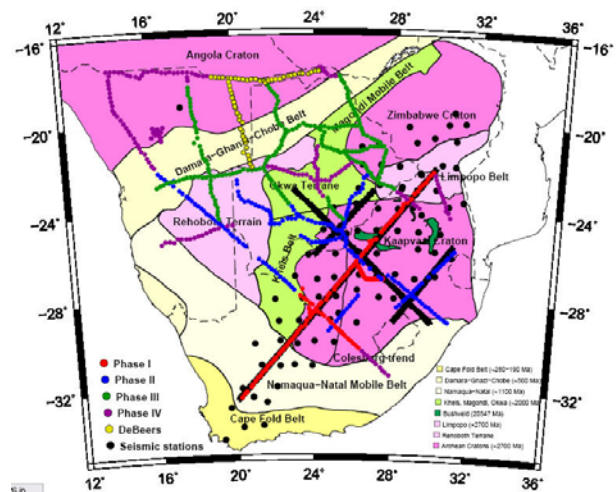


Figure 1: Locations of the SASE (black dots) and SAMTEX (coloured dots) stations. The background is the tectonic subdivision of Southern Africa by Webb.

We show that the empirically-derived relationship between shear-wave velocity (V_s) and electrical

resistivity (ρ) is consistent with laboratory-derived relationships, and that predicting the lithospheric V_s velocity from electrical resistivity is valid for most of Southern Africa to within ± 0.1 km/s.

QUALITATIVE COMPARISONS

The resistivity images at 100 km and 200 km are discussed in the Jones et al. SAGA abstract. For the velocity models, we take two published models and one unpublished one. Two of these are surface wave (SW) models, whereas the third is a body wave (BW) model.

1) Resistivity models

The resistivity models at 100 km and 200 km are shown in Figs. 2 and 3 below for completeness.

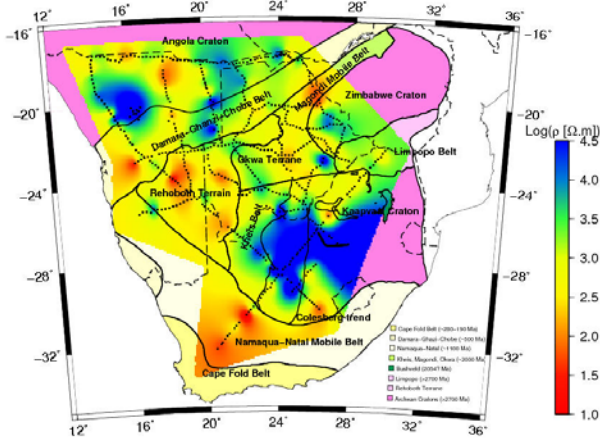


Figure 2: An image of the resistivity at 100 km depth based on an approximate transformation of the MT responses from period to depth and taking the maximum resistivity found. The colours are $\log_{10}(\text{resistivity})$, and the black dots show stations at which data were used. At the P-T conditions for the Kaapvaal Craton mantle rocks at 100 km depth comprising olivine, pyroxenes and garnet are expected to have a resistivity in excess of 30,000 ohm.m, i.e., blue.

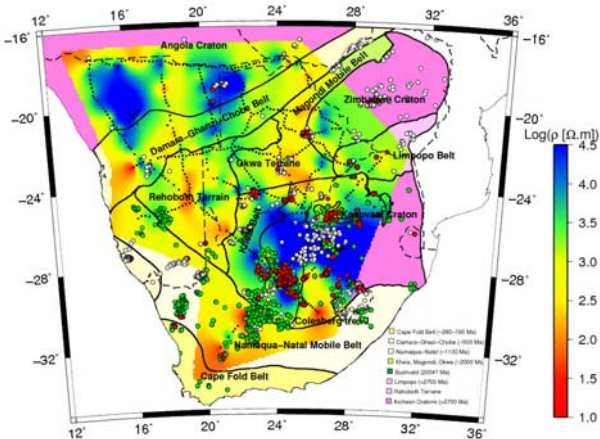


Figure 3: An image of the resistivity at 200 km constructed in the same manner as Fig. 2. Also shown on the figure are kimberlite locations; red means known to be diamondiferous, green means known to be non-diamondiferous, and white means not defined or unknown. At the P-T conditions for the Kaapvaal Craton mantle

rocks at 100 km depth comprising olivine, pyroxenes and garnet are expected to have a resistivity in excess of 1,000 ohm.m, i.e., green to blue.

2) Li and Burke SW model

As shown by Li and Burke (2006), the sensitivity kernels for surface wave methods are such that the deeper in the Earth one investigates, the more smearing occurs due to the broadening of the kernels. Figure 5 of Li and Burke (2006) shows that the resolution kernel for 50 s periodicity is centred on 80 km, and averages information from approximately the base of the crust (40 km) to approximately the graphite-diamond phase transition (140 km), thus this depth gives a weighted average of the 1-D vertical seismic velocity in the upper lithospheric mantle.

Figure 4 shows the velocities in the 80-100 km depth slice of the Li and Burke SW model, and can be directly compared qualitatively with the corresponding resistivity map at 100 km (see Jones et al. SAGA abstract). Also plotted on the figure are the kimberlite localities. As with electrical resistivity, there is a positive correlation of diamondiferous kimberlites with the edge of the high velocity body associated with the Kaapvaal Craton and also with the edge of the high velocity body associated with the Zimbabwe Craton.

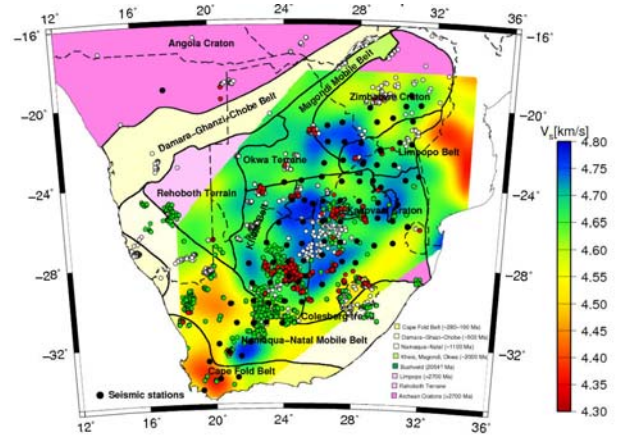


Figure 4: Shear wave seismic velocity at a depth of 100 km from a model constructed through inversion of fundamental mode Rayleigh wave arrivals into the SASE array (Li and Burke 2006). Also shown on the figure are kimberlite locations; red means known to be diamondiferous, green means known to be non-diamondiferous, and white means not defined or unknown.

Performing a cross-plot between $\text{Log}_{10}(\rho)$ and V_s we obtain Fig. 5, where the velocity of the closest node to each MT station was taken, with a maximum station separation of 50 km.

Assuming both data are in error (Fasano and Vio 1988, York 1966, 1969), and performing a linear regression with robust outlier rejection (Huber 1981), yields the result that V_s velocity and electrical resistivity at 100 km are related by:

$$V_{S100} = 4.50 + 0.045 * \text{Log}_{10}(\rho_{100} [\text{ohm.m}]) \text{ km/s.}$$

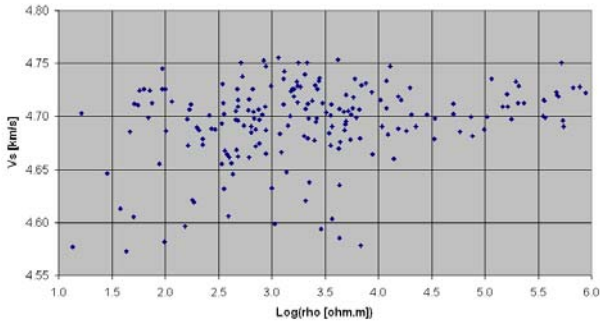


Figure 5: cross-plot between electrical resistivity and shear wave velocity at 100 km beneath Southern Africa.

Departures from this relationship are predominantly in Botswana, where there are a large number of high velocity-medium resistivity values where the velocity model is poor due to lack of station coverage.

3) Fouch BW models

The Vp and Vs perturbation anomaly maps at 200 km from the Fouch et al. (2004) body wave models are shown in Figs 6 and 7 respectively, together with the resistivity map at that same depth and the kimberlite information. Velocity anomalies in the range ±0.25% are set to transparent, and positive velocity anomalies grade through blue to black (1.25%) and negative ones grade through red to black (-1.25%).

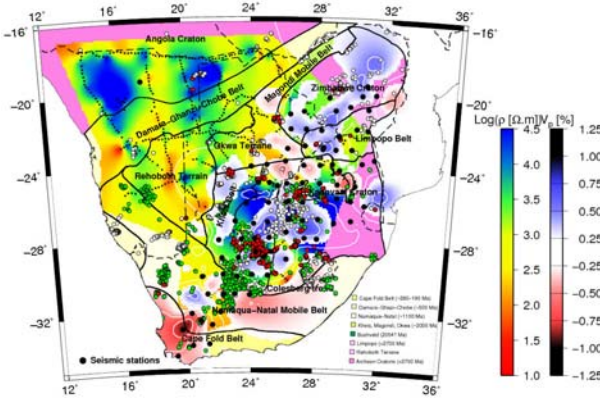


Figure 6: Comparison of the resistivity image at 200 km with the anomalous compressional velocities from models constructed through inversion of body wave arrivals (Fouch, et al. 2004, James, et al. 2001). The resistivities are plotted in log10(resistivity), and the velocity perturbations are in terms of percentage difference from the average at that depth, with values between -0.25% and +0.25% set to transparent. Kimberlite locations plotted with the same colour coding as Fig. 2.

As with the Li and Burke map (Fig. 4), there is an obvious correlation of the boundaries of the high velocity anomaly associated with the Kaapvaal Craton. The fast velocity anomalies in both Vp and Vs spatially correlate well with high resistivity anomalies, and vice-versa. The one region that appears to contradict this central Botswana, which displays a low resistivity

region no Vp anomaly (Fig. 6), but a relatively strong (0.5%) fast Vs anomaly (Fig. 7).

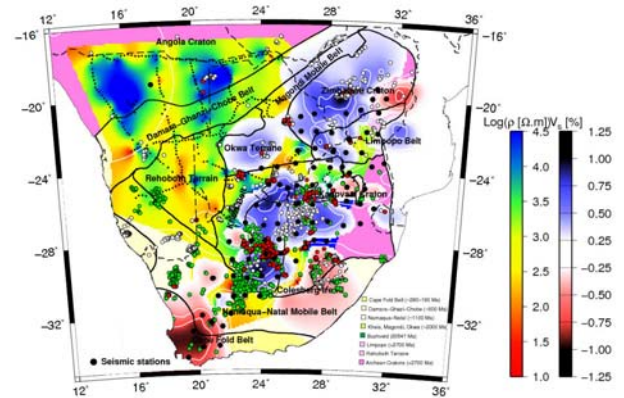


Figure 7: Comparison of the resistivity image at 200 km with the anomalous shear wave velocities from models constructed through inversion of body wave arrivals (Fouch, et al. 2004, James, et al. 2001). The resistivities are plotted in log10(resistivity), and the velocity perturbations are in terms of percentage difference from the average at that depth, with values between -0.25% and +0.25% set to transparent. Kimberlite locations plotted with the same colour coding as Fig. 2.

4) Fishwick SW model

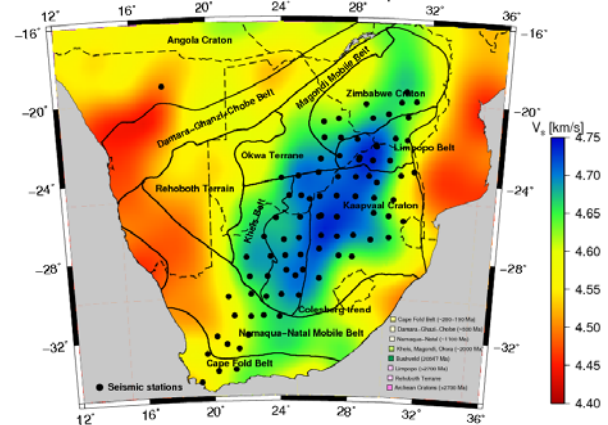


Figure 8: Vs velocity at 100 km from Fishwick SW inversion.

Fishwick has derived a regional model for Africa, using the SASE data for higher resolution in Southern Africa. The tomographic inversion is described in Fishwick et al. (2008), and comprises a two-stage approach with (1) derivation of path-averaged models based on the Debayle method from the fundamental Rayleigh wave and first four higher modes for data in the period range 50-120 s, then (2) depth slices calculated using path averaged velocities with the tomographic inversion code of Yoshizawa, first with 6 degree knot points then reducing to 1.5 degree for detailed structure. The 100 km depth slice for the region of interest is shown in Fig. 8. To compare this map with the resistivity image in Fig. 2, the resistivity map must be treated with the same

smoothing, i.e., 1.5 degree instead of the 0.5 degree used, which results in the map shown in Fig. 9.

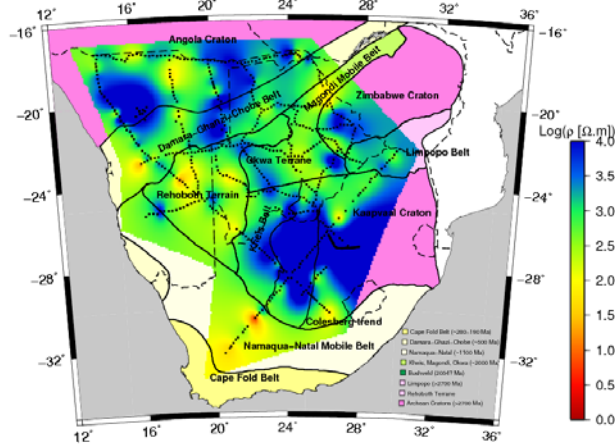


Figure 9: Resistivity map at 100 km smoothed with 1.5 deg filter for comparison with Fishwick's Vs model (Fig. 9).

QUANTITATIVE COMPARISON

Assuming that the physical properties of the lithospheric mantle are a function of known parameters one can create “rocks” numerically using the laboratory-derived empirical relationships for single minerals coupled with an appropriate mixing theory. Jones et al. (2009) recently provided an extremal bounds approach for deriving seismic compressional and shear velocities, density and electrical conductivity of mineral assemblages assuming that temperature, pressure, iron content and composition are known, and that the individual mineral species are olivine, ortho- and clinopyroxene and garnet. This approach has merit in that the limits derived for the physical parameters represent plausible bounds within which the “true” values must lie.

Taking the parameters of the middle of the Kaapvaal Craton mantle lithosphere beneath Kimberley, namely:

- Depth = 150 km
- Temperature = 1010 °C
- Pressure = 4.63 GPa
- Mg# = 91.0
- Olivine = 65%
- Orthopyroxene = 26.9%
- Clinopyroxene = 6.1%
- Garnet = 1.3%

(see Jones, et al. 2009 for details) and using the formulae and extremal bounds approach in Jones et al. (2009) we obtain the following geometric means and ranges of physical properties of the mineral assemblage:

- Vp = 8.16 (8.13 – 8.18) km/s,
- Vs = 4.56 (4.55 – 4.57) km/s,
- Density = 3.32 gm/cm³,
- Log(resistivity) = 3.69 (3.64 – 3.71) (ohm.m).

Varying only temperature, from 700 °C to 1300 °C, and keeping all other parameters constant, we find a

relationship between Log(resistivity) and Vs as shown in Fig. 10 (black line). This curvilinear line can be fit to a first approximation to a linear regression (red line in Fig. 10) between Log(resistivity) and Vs given by:

$V_{S150} = 4.200 + 0.09602 * \text{Log}_{10}(\rho_{150} [\text{ohm.m}]) \text{ km/s}$, which describes the region around 1000 °C well, but not the whole temperature range. Using a quadratic regression, we obtain an excellent model fit of

$$V_{S150} = 3.942 + 0.2317 * \text{Log}_{10}(\rho_{150}) - 0.01708 * (\text{Log}_{10}(\rho_{150}))^2 \text{ km/s}$$

(the predicted Vs is not shown on Fig. 10 as it lies on top of the observed curve) valid for the temperature range of 700 °C to 1300 °C and a depth of 150 km.

Focussing on the temperature region around 1010 °C and performing a linear regression for the range 960-1060 °C, the relationship is:

$$V_{S150} = 4.184 + 0.1032 * \text{Log}_{10}(\rho_{150} [\text{ohm.m}]) \text{ km/s}$$

which can be used as a first-approximation.

Performing this exercise at temperatures and pressures of (740 °C, 3.00 GPa) and (1250 °C, 6.28 GPa), which are the estimated temperatures and pressures at 100 km and 200 km respectively beneath Kimberley, we obtain:

$$V_{S100} = 4.296 + 0.06216 * \text{Log}_{10}(\rho_{100} [\text{ohm.m}]) \text{ km/s},$$

and

$$V_{S200} = 4.140 + 0.1429 * \text{Log}_{10}(\rho_{200} [\text{ohm.m}]) \text{ km/s}.$$

The quadratic expressions for broader temperature ranges are:

$$V_{S100} = 3.831 + 0.2457 * \text{Log}_{10}(\rho_{100}) - 0.01801 * (\text{Log}_{10}(\rho_{100}))^2 \text{ km/s},$$

and

$$V_{S200} = 3.949 + 0.2782 * \text{Log}_{10}(\rho_{200}) - 0.02406 * (\text{Log}_{10}(\rho_{200}))^2 \text{ km/s}.$$

Either the depth-dependent quadratic expressions for broad temperature variation, or individual linear expressions for narrower (± 50 °C) temperature variation, can be used to predict Vs from $\text{Log}_{10}(\rho)$.

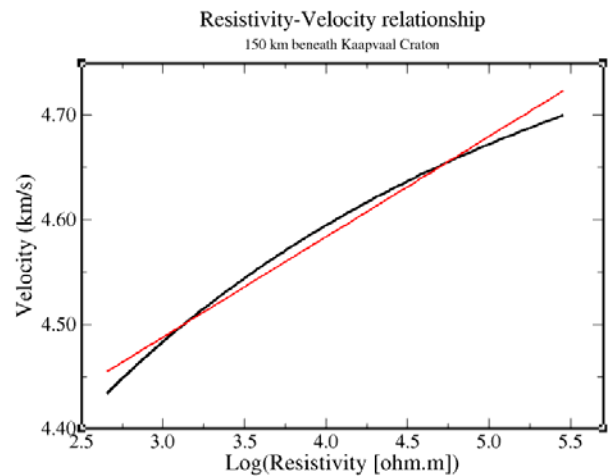


Figure 10: Log₁₀(resistivity)-velocity cross-plot from laboratory predictions

Note that the relationship defined between the Li and Burke model velocities at 100 km and the 100 km resistivities from the approximate imaging was:

$$V_{S100} = 4.50 + 0.045 * \text{Log}_{10}(\rho_{100} [\text{ohm.m}]) \text{ km/s,}$$

which compares well with the laboratory-defined mineral physics prediction above for V_{S100} .

A cross-plot of the weakly smoothed Log_{10} (resistivity) (Fig. 2) and V_s velocity (Fig. 8) at 100 km from Fishwick's model is shown in Fig. 11, together with the mineral physics prediction for V_{S100} from ρ_{100} given by the quadratic expression above.

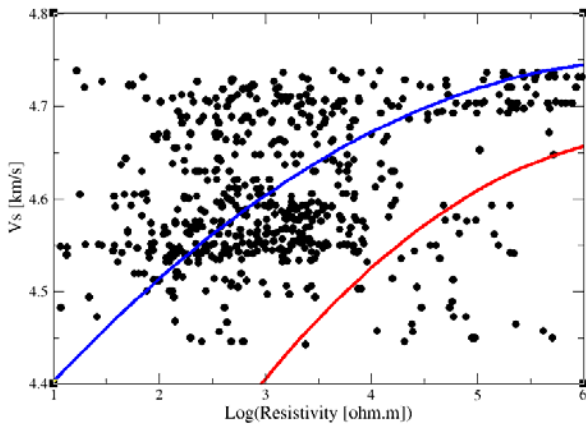


Figure 11: V_s -rho cross-plot for Figs. 2 (raw resistivities) and 8 (Fishwick SW model velocities) together with the mineral physics prediction for 100 km depth (red line) and the adjusted correlation (blue line).

The mineral physics prediction (red line in Fig. 11) clearly does not explain the data – there is a systematic bias towards higher velocities/lower resistivities. Assuming that the mineral physics is correct, which is questioned by Jones et al. (Jones, et al. 2009), then the bias exists in the estimation of velocity and/or resistivity. A bias is in MT when estimating the resistivity of a resistive layer sandwiched between two conducting ones, which is the situation for the upper half of the SCLM (Jones 1999). The *shape* of the log(resistivity)-velocity relation is likely correct, but the level may be in error due to bias. Moving the mineral physics regression to less resistive values to correct for the bias (blue line in Fig. 10), one can obtain visually a fit to the data. The empirical relationship between V_s and $\log(\rho)$ at 100 km is given approximately by:

$$V_{S100} = 4.27 + 0.14 * \text{Log}_{10}(\rho_{100}) - 0.011 * (\text{Log}_{10}(\rho_{100}))^2 \text{ km/s.}$$

This relationship can be tested by looking for departures from the trend line (blue line in Fig. 11). White means that the data point is within 25% of the trend line (within ± 0.05 km/s equivalent), whereas blue means the region is slower/more resistive than consistent, and red means faster/less resistive than consistent.

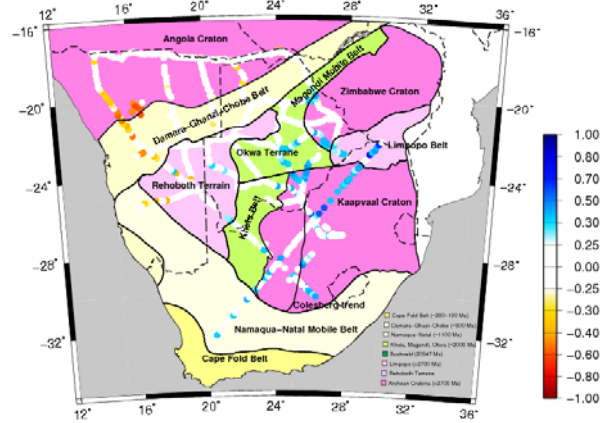


Figure 12: Departures from the blue trend line in Fig. 10.

There are two regions where the data are consistently off the blue trend line, namely NW Namibia (red) and NE South Africa (blue) – these two regions are essentially all of the points in the bottom right (high resistivity/low velocity; NW Namibia) and top left (low resistivity/high velocity; NE South Africa) corners of Fig. 10. The latter is likely explained by the presence of some conducting phase within the lithosphere beneath that region that was introduced as part of Bushveld magmatism. The former is far more difficult to explain – it is easy to make rocks more conductive than expected, but virtually impossible to make them more resistive, so that region must be seismically slower than the electrical resistivities predict.

Finally, given the blue trend line and the resistivities and velocities at 100 km, one can compare the observed velocities with those predicted from electrical resistivity. The difference map between $(V_s)_{\text{observed}}$ and $(V_s)_{\text{predicted}}$ is shown in Fig. 13, with regions where the difference is < 0.05 km/s made transparent, and regions with differences in the range 0.05-0.10 km/s shaded in light blue (faster) or red (slower).

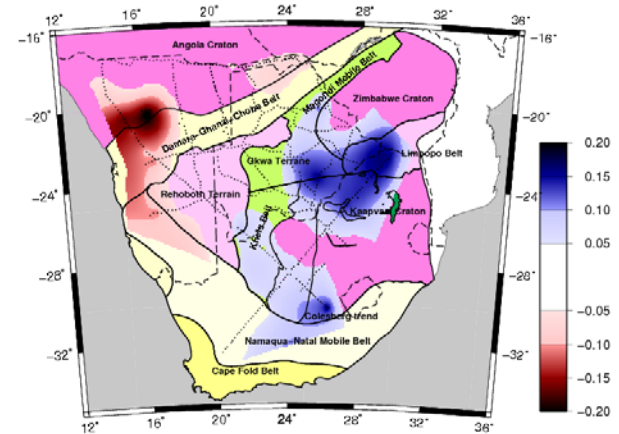


Figure 13: Difference map between V_s observed (Fig. 8) and V_s predicted from mineral physics regression applied to resistivities (Fig. 2).

The regions of differences >0.10 km/s are, not surprisingly, those identified in Fig. 12. What is astounding is that for most of Southern Africa, apart from two regions, there is a definable quantitative relationship between shear wave velocity and the logarithm of electrical resistivity.

We note that the higher resolution SW model of Li and Burke (2006) and the BW models of Fouch et al. (2004) for the SASE array have slower velocities in the NE part of South Africa, and would correlate better with the reduced resistivities than does the regional model of Fishwick.

CONCLUSIONS

Combining seismic and electrical data and information about the Sub-Continental Lithospheric Mantle (SCLM) unequivocally adds to our knowledge of lithospheric processes – the whole is far greater than the sum of the parts. Herein we have not undertaken a formal linking between the two, such as that performed in joint inversion by Moorkamp et al. (2007), but have demonstrated that for much of Southern Africa seismic velocities and electrical resistivities are correlated to a very high degree, and that the correlation can be described quantitatively. The exact relationship between $\log(\text{resistivity})$ and velocity needs refining, including superior estimates of both velocity and resistivity, and the inference from mineral physics is that a quadratic relationship is appropriate.

The implications of this observation are far reaching – electrical resistivity variation in mantle minerals likely to constitute the SCLM is almost entirely due to temperature variation (Jones, et al. 2009), whereas for velocities (both compressional and shear) temperature account for about 75% of the effect and the remaining 25% is due to compositional variation. Combining the two is a way of removing the temperature effect from velocities and leaving compositional variation. It is possible that the slow region identified in NW Namibia that is inconsistent with the resistivities observed may have strong compositional differences compared to the rest of Southern Africa.

Also, in reverse that electrical resistivity is so well correlated with seismic velocity and maps onto the mineral physics prediction means that there are few regions with resistivity reduction due to exotic anomalies, such as the Central Slave Mantle Conductor (CSMC) in the middle of the Slave Craton's SCLM (Jones, et al. 2001, 2003). The one anomalously conducting region is NE South Africa, where the resistivities are lower than predicted from the velocities. This may be due to conducting phases in the mantle lithosphere introduced during Bushveld magmatism, but also the velocities from the regional model of Fishwick may be too high and the lower ones in the models of Li

and Burke (2006) and Fouch et al. (2004) more accurate.

ACKNOWLEDGMENTS

Many, many, many people on three continents contributed to the huge achievement in data acquisition of the SAMTEX project. Besides the consortium members and their staffs, we wish to acknowledge Phoenix Geophysics' many timely contributions of equipment and spares, and the Geological Survey of Canada and the U.S. Electromagnetic Studies of Continents consortium (EMSOC) for access to instrumentation for Phase I. We especially thank our academic funding sponsors; the Continental Dynamics programme of the U.S. National Science Foundation, the South African Department of Science and Technology, and Science Foundation Ireland, and our industry sponsors; De Beers, RTME, BHP-B and ABB.

Finally, we thank the people of Southern Africa for their generous warm spirit allowing weird scientists on their land.

REFERENCES

- Fasano, G., and Vio, R., 1988, Fitting a Straight Line with Errors on Both Coordinates. *Newsletter of Working Group for Modern Astronomical Methodology* **7**, 2-7.
- Fishwick, S., Heintz, M., Kennett, B.L.N., A.M., R., and Yoshizawa, K., 2008, Steps in Lithospheric Thickness within Eastern Australia, Evidence from Surface Wave Tomography. *Tectonics* **27**.
- Fouch, M.J., James, D.E., VanDecar, J.C., van der Lee, S., and Kaapvaal Seismic, G., 2004, Mantle Seismic Structure beneath the Kaapvaal and Zimbabwe Cratons. *South African Journal of Geology* **107**, 33-44.
- Huber, P.J., 1981, *Robust Statistics*. John Wiley, New York.
- James, D.E., Fouch, M.J., VanDecar, J.C., van der Lee, S., and Kaapvaal Seismic, G., 2001, Tectospheric Structure beneath Southern Africa. *Geophysical Research Letters* **28**, 2485-88.
- Jones, A.G., 1999, Imaging the Continental Upper Mantle Using Electromagnetic Methods. *Lithos* **48**, 57-80.
- Jones, A.G., Evans, R.L., and Eaton, D.W., 2009, Velocity-Conductivity Relationships for Mantle Mineral Assemblages in Archean Cratonic Lithosphere Based on a Review of Laboratory Data and Application of Extremal Bound Theory. *Lithos* **109**, 131-43.
- Jones, A.G., Ferguson, I.J., Chave, A.D., Evans, R.L., and McNeice, G.W., 2001, The Electric Lithosphere of the Slave Craton. *Geology* **29**, 423-26.

- Jones, A.G., Lezaeta, P., Ferguson, I.J., Chave, A.D., Evans, R.L., Garcia, X., and Spratt, J., 2003, The Electrical Structure of the Slave Craton. *Lithos* **71**, 505-27.
- Li, A.B., and Burke, K., 2006, Upper Mantle Structure of Southern Africa from Rayleigh Wave Tomography. *Journal of Geophysical Research-Solid Earth* **111**, 16.
- Moorkamp, M., Jones, A.G., and Eaton, D.W., 2007, Joint Inversion of Teleseismic Receiver Functions and Magnetotelluric Data Using a Genetic Algorithm: Are Seismic Velocities and Electrical Conductivities Compatible? *Geophysical Research Letters* **34**.
- York, D., 1966, Least-Squares Fitting of a Straight Line. *Canadian Journal of Physics* **44**, 1079-86.
- , 1969, Least Squares Fitting of a Straight Line with Correlated Errors. *Earth and Planetary Science Letters* **5**, 320-24.